

Insights into the Relationship Between D- and A-optimal Designs

Andrew T. Karl*

Bradley Jones†

Abstract

For a fixed linear-model basis, we show that the A criterion factors into an inverse- D scale term and a dimensionless sphericity factor that depends only on eigenvalue dispersion. This factor isolates exactly the part of A not controlled by the determinant, explaining why designs that are exact or near ties in D can differ materially in coefficient-variance, aliasing, and prediction-variance behavior. We illustrate the factorization on a published D tie and on screening settings with infinitely many D -optimal solutions, then use the same scale/shape viewpoint as a lightweight post-screen within a space-filling candidate pool. A final section connects the same idea to Kiefer’s Φ -class and introduces sphericity profiles.

Keywords: sphericity index; eigenvalue dispersion; screening experiments; space-filling designs; MaxPro.

1 Introduction

Consider the full-rank linear model $Y = X\beta + \varepsilon$ with $\text{Var}(\varepsilon) = \sigma^2 I_n$. The least squares estimator satisfies $\text{Var}(\hat{\beta}) = \sigma^2(X^\top X)^{-1}$. The classical D and A criteria are

$$D(X) = \{\det(X^\top X)\}^{1/p}, \quad A(X) = \text{tr}\{(X^\top X)^{-1}\}, \quad (1)$$

where p is the number of model parameters (columns of X). Because σ^2 is common across designs, we suppress that multiplicative factor when comparing coefficient and prediction variances; multiplying the quantities below by σ^2 recovers the corresponding variances. For notational convenience, write $C = X^\top X$ for the information matrix. We will express the criteria primarily through the spectra of C and C^{-1} . If s_1, \dots, s_p are the singular values of X , then the information eigenvalues are s_i^2 and the covariance eigenvalues are s_i^{-2} , so the same quantities can also be obtained directly from an SVD of X without explicitly forming $X^\top X$. This eigenvalue/SVD viewpoint is convenient computationally and aligns directly with the geometry of confidence ellipsoids and with the covariance-spectrum displays used later in the paper.

In screening experiments the inferential goal is typically identification of active effects, so criteria tied directly to coefficient variances (such as A) are naturally aligned with the objective; this motivation underlies the screening-focused comparisons of Jones et al. (2021). A recurring practical issue is that D can have many exact (or near) ties, and these ties can differ materially under other diagnostics. For example, Jones et al. (2021) report a screening example in which the published A -optimal and D -optimal designs are an exact tie in D but differ in aliasing and prediction-variance diagnostics (including the G criterion). Similarly, Stallrich et al. (2023) show that in some screening settings there can be infinitely many D -optimal designs with different variance properties; they note that this situation “is cause for concern about the D -criterion’s ranking of screening designs”.

*Karl Statistical Services LLC, Aurora, CO, USA. Email: akarl@asu.edu. ORCID: 0000-0002-5933-8706.

†Independent Consultant, Cary, NC, USA.

We give a compact explanation. We show that A admits a clean factorization into an inverse- D scale term multiplied by a scale-free sphericity term that depends only on spectral balance. The resulting sphericity index is exactly the part of A that can distinguish D ties. We also show how the same scale/shape viewpoint can be used as a lightweight post-screen that adds a working-model preference within a space-filling candidate pool while keeping the spacing criterion primary.

Section 2 introduces notation and derives the A factorization into an inverse-determinant scale term and a scale-free sphericity index, along with a geometric interpretation in terms of confidence ellipsoids. Section 3 revisits a published D tie from Jones et al. (2021). Section 4 discusses an example with infinitely many D -optimal screening designs from Stallrich et al. (2023). Section 5 proposes a practical post-screen for space-filling candidate pools by combining a spacing score with working-model sphericity. Section 6 connects the same scale/shape separation to Kiefer’s Φ -class and uses sphericity profiles as a continuous shape diagnostic linking D and A .

2 Scale and sphericity in A-optimality

2.1 Notation and spectral conventions

Let $C = X^\top X$ denote the $p \times p$ information matrix. Let $\mu_1, \dots, \mu_p > 0$ denote the eigenvalues of C , and let $\lambda_1, \dots, \lambda_p > 0$ denote the eigenvalues of the covariance matrix C^{-1} , so that $\lambda_i = \mu_i^{-1}$. If $s_1, \dots, s_p > 0$ are the singular values of X , then $\mu_i = s_i^2$ and $\lambda_i = s_i^{-2}$. When we display covariance spectra we sort the values in decreasing order and write $\lambda_{(1)} \geq \dots \geq \lambda_{(p)}$. We assume X has full column rank, so $\mu_i > 0$.

For a positive vector $v = (v_1, \dots, v_p)$, define the arithmetic, geometric, and harmonic means by

$$\text{AM}(v) := \frac{1}{p} \sum_{i=1}^p v_i, \quad \text{GM}(v) := \left(\prod_{i=1}^p v_i \right)^{1/p}, \quad \text{HM}(v) := \frac{p}{\sum_{i=1}^p v_i^{-1}}.$$

Define the D scale,

$$D(X) = \{\det(C)\}^{1/p} = \text{GM}(\mu), \tag{2}$$

and note that

$$A(X) = \text{tr}(C^{-1}) = \sum_{i=1}^p \lambda_i = p \text{AM}(\lambda). \tag{3}$$

Equivalently, since the eigenvalues of C^{-1} are $\{\mu_i^{-1}\}$,

$$A(X) = \sum_{i=1}^p \mu_i^{-1} = \frac{p}{\text{HM}(\mu)}. \tag{4}$$

Thus D is a geometric-mean information scale, while A is proportional to an arithmetic-mean covariance scale (or, equivalently, the reciprocal of the harmonic mean of the information eigenvalues). Some authors instead define the A -criterion as the average variance per parameter, $\bar{A}(X) := \frac{1}{p} \text{tr}(C^{-1}) = \text{AM}(\lambda)$.

2.2 A sphericity index and a factorization of A

Define the sphericity index

$$\mathcal{S}(C) := \left\{ \frac{\det(C^{-1})}{(\text{tr}(C^{-1})/p)^p} \right\}^{1/p} = \frac{p}{\text{tr}(C^{-1}) \{\det(C)\}^{1/p}} = \frac{p}{A(X)D(X)}, \quad 0 < \mathcal{S}(C) \leq 1. \tag{5}$$

Equivalently,

$$\mathcal{S}(C) = \frac{\det(C^{-1})^{1/p}}{\text{tr}(C^{-1})/p} = \frac{\text{GM}(\lambda)}{\text{AM}(\lambda)} = \frac{\text{HM}(\mu)}{\text{GM}(\mu)}.$$

The bound $0 < \mathcal{S}(C) \leq 1$ follows from $\text{GM}(\lambda) \leq \text{AM}(\lambda)$, with equality if and only if $\lambda_1 = \dots = \lambda_p$. The index \mathcal{S} is dimensionless and scale invariant: for any $c > 0$, $\mathcal{S}(cC) = \mathcal{S}(C)$. Thus \mathcal{S} depends only on spectral balance, that is, on how far the covariance spectrum is from being flat.

In multivariate analysis, the determinant–trace sphericity index (Mauchly’s W) is

$$W = \frac{\det(C^{-1})}{(\text{tr}(C^{-1})/p)^p},$$

so $\mathcal{S}(C) = W^{1/p}$ (Mauchly, 1940; Nagarsenker and Pillai, 1973).

All comparisons of \mathcal{S} are intended under a fixed working-model basis and coding convention; rescaling columns of X changes the spectrum of C and therefore changes shape summaries (Goos, 2002). In screening applications it is customary to scale each quantitative factor to a common range (e.g., $[-1, 1]$), so the coding is typically fixed before comparing designs.

Rearranging (5) yields the factorization

$$\boxed{A(X) = \frac{p}{D(X)} \frac{1}{\mathcal{S}(C)}}. \tag{6}$$

This identity makes explicit that A is an inverse- D scale multiplied by a pure-shape penalty $1/\mathcal{S}$. In particular, among exact D -ties (or near ties where $\det(C)$ varies little), differences in A are driven entirely by \mathcal{S} .

2.3 An upper bound on relative prediction variance

Prediction behavior can be summarized by the relative prediction-variance function

$$v(x) := f(x)^\top C^{-1} f(x), \quad x \in \mathcal{X},$$

where $f(x)$ is the p -vector of model terms evaluated at x and \mathcal{X} denotes the design region. The actual prediction variance is $\sigma^2 v(x)$. Define the G value by

$$G(X) := \max_{x \in \mathcal{X}} v(x),$$

so G -optimality minimizes $G(X)$ (Myers et al., 2016). For any x , an upper bound on the relative prediction variance is

$$v(x) \leq \lambda_{\max}(C^{-1}) \|f(x)\|^2 \leq \text{tr}(C^{-1}) \|f(x)\|^2 = A(X) \|f(x)\|^2 = \frac{p}{D(X)} \frac{1}{\mathcal{S}(C)} \|f(x)\|^2,$$

where the first inequality is the Rayleigh quotient bound and the second uses $\lambda_{\max}(C^{-1}) \leq \text{tr}(C^{-1})$ (see, e.g., Harville, 1997). Thus, for a fixed working model and region (so $\|f(x)\|$ is bounded under standard coding), $1/\mathcal{S}(C)$ acts as a pure-shape penalty that tightens or loosens an envelope on worst-case prediction variance.

2.4 Connection to JMP Evaluate Design efficiencies

In JMP's Evaluate Design platform, the reported D , A , and G metrics are efficiencies relative to an ideal orthogonal design (SAS Institute Inc., 2025). To avoid confusion with the determinant scale $D(X) = \det(X^\top X)^{1/p}$, we denote these by D_{eff} , A_{eff} , and G_{eff} . Because these quantities depend on the chosen model matrix, all reported efficiencies and \mathcal{S} values are computed under the stated working model. With X the $n \times p$ model matrix (including an intercept column when present), JMP defines

$$D_{\text{eff}} = 100 \frac{\det(X^\top X)^{1/p}}{n}, \quad A_{\text{eff}} = 100 \frac{p}{n \operatorname{tr}\{(X^\top X)^{-1}\}}, \quad G_{\text{eff}} = 100 \frac{p}{n \max_{x \in \mathcal{X}} v(x)}, \quad (7)$$

where $v(x) = f(x)^\top (X^\top X)^{-1} f(x)$ is the relative prediction variance at x , $f(x)$ is the p -vector of model terms evaluated at x , and \mathcal{X} is the design region. (G_{eff} is computed using Monte Carlo sampling of the region.) Combining (7) with (5) yields the identity

$$A_{\text{eff}} = D_{\text{eff}} \mathcal{S}(C), \quad \text{equivalently} \quad \mathcal{S}(C) = \frac{A_{\text{eff}}}{D_{\text{eff}}}, \quad (8)$$

which makes the scale/shape separation visible directly in the reported efficiencies.

2.5 Geometric interpretation: overall scale versus roundness

The $100(1 - \alpha)\%$ joint confidence ellipsoid for β has the form

$$E = \left\{ \beta : (\beta - \hat{\beta})^\top C (\beta - \hat{\beta}) \leq \kappa \right\}, \quad \kappa := p \hat{\sigma}^2 F_{p, n-p; 1-\alpha},$$

where $\hat{\sigma}^2$ is the usual residual-variance estimator (Myers et al., 2016). The eigenstructure of $C = X^\top X$ determines both the overall size of E and its roundness.

Writing

$$C = U \operatorname{diag}(\mu_1, \dots, \mu_p) U^\top, \quad \mu_i > 0,$$

the principal axes of E are aligned with the columns of U and have semi-axis lengths $\sqrt{\kappa/\mu_i}$. Equivalently, if λ_i are the eigenvalues of C^{-1} (so $\lambda_i = 1/\mu_i$), the semi-axis lengths are $\sqrt{\kappa \lambda_i}$.

The D criterion controls an overall scale (volume) aspect of the ellipsoid. Up to a constant depending only on (p, α) ,

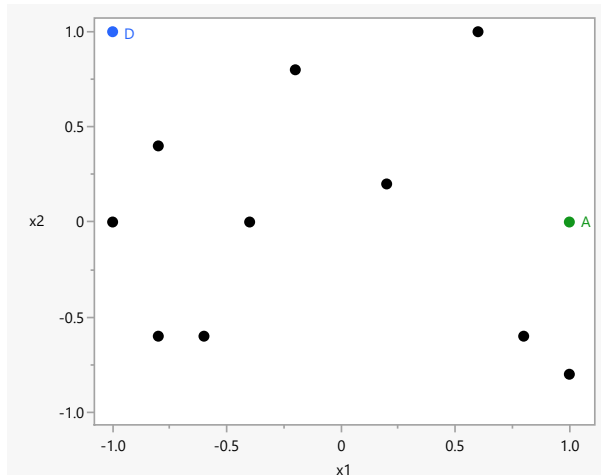
$$\operatorname{Vol}(E) \propto \prod_{i=1}^p \sqrt{\kappa/\mu_i} = \kappa^{p/2} \det(C)^{-1/2}.$$

Thus maximizing $\det(C)$ shrinks the joint uncertainty region in a multiplicative (geometric-mean) sense (Myers et al., 2016), and the factorization

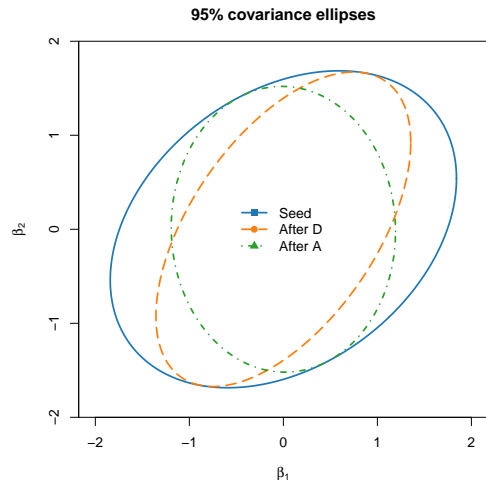
$$\operatorname{tr}(C^{-1}) = \frac{p}{\mathcal{S}(C)} \det(C^{-1})^{1/p}$$

shows that A -optimality penalizes spectral imbalance via the factor $1/\mathcal{S}(C)$ while still depending on determinant scale through $\det(C^{-1})^{1/p}$.

Figure 1 gives a one-step augmentation illustration in two factors under a quadratic response-surface working basis. Starting from a fixed $n = 10$ seed design (black points), we add one run by D -optimality or by A -optimality under the same working basis (Figure 1a). Figure 1b compares the resulting 95% covariance ellipses for the two linear coefficients (β_1, β_2) , up to the common factor σ^2 ,



(a) Seed design with A - and D -optimal augmentation points.



(b) Covariance ellipses for (β_1, β_2) .

Figure 1: One-step augmentation illustration.

Augmented design	D_{eff}	A_{eff}	G_{eff}	$\mathcal{S}(C)$	$p/D(X)$
A -optimal augmentation	23.03	13.24	16.56	0.575	2.37
D -optimal augmentation	24.25	11.25	16.13	0.464	2.25

Table 1: One-step augmentation summary (Figure 1).

based on the corresponding 2×2 principal submatrix of $(X^\top X)^{-1}$. Table 1 reports the associated scale/shape summaries.

The A -optimal augmentation yields the rounder covariance ellipse in Figure 1b. Its D_{eff} is only modestly lower than that of the D -optimal augmentation (23.03 versus 24.25), while its A_{eff} and sphericity are materially better (13.24 versus 11.25, and 0.575 versus 0.464), and its G_{eff} is slightly better as well. In this example, the small sacrifice in determinant scale appears worthwhile for the gain in roundness.

3 A published D tie in screening designs

Jones et al. (2021) give screening examples in which A - and D -optimal designs differ, and also examples where distinct D -optimal designs behave differently under other diagnostics. In their Example 2 (main-effects working model), the reported A -optimal and D -optimal designs are an exact tie in D . We report D_{eff} , A_{eff} , and G_{eff} as relative efficiencies reported by JMP (larger is better). Table 2 reports the corresponding sphericity indices \mathcal{S} ; the design with larger \mathcal{S} is the A -optimal design.

Figure 2a summarizes the covariance spectrum via the normalized eigenvalue shares

$$q_i := \frac{\lambda_i}{\sum_{j=1}^p \lambda_j}, \quad \sum_i q_i = 1, \quad (9)$$

and plots the ordered values $q_{(1)} \geq \dots \geq q_{(p)}$. Holding D fixed, a more uniform ordered spectrum (larger \mathcal{S}) yields smaller A through (6).

Design	D_{eff}	A_{eff}	G_{eff}	$\mathcal{S}(C)$	$p/D(X)$
A-optimal	96.70	94.12	57.14	0.973	0.69
D-optimal	96.70	91.43	40.00	0.945	0.69

Table 2: Jones et al. (2021, Example 2): relative efficiencies and sphericity for a D tie.

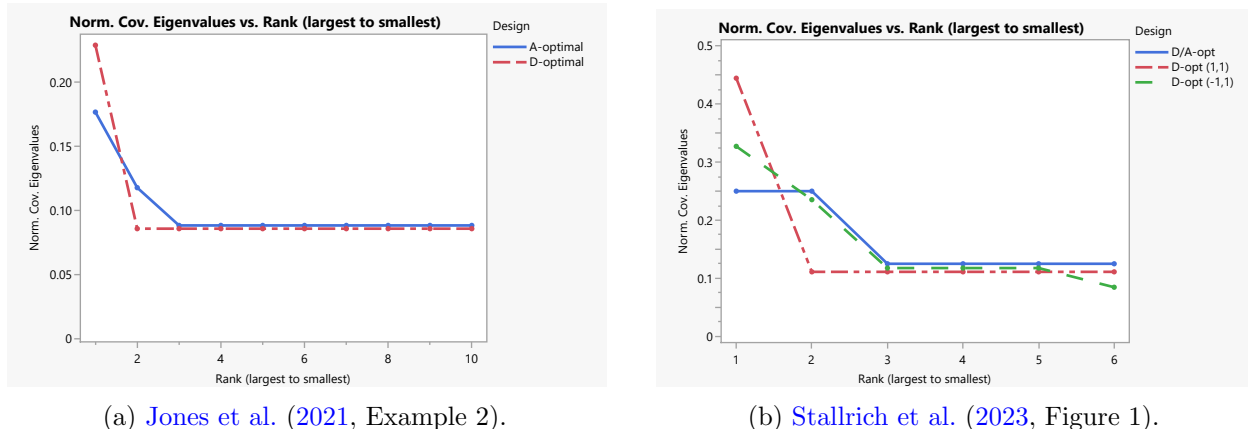


Figure 2: Ordered normalized covariance spectra.

The practical difference is substantial. Although the two designs tie in D_{eff} , the A -optimal design has better A_{eff} and markedly better G_{eff} . Figure 2a shows why: the A -optimal design spreads covariance more evenly across directions, whereas the competing D tie concentrates more mass in the largest covariance direction. That flattening is exactly what the larger sphericity index records.

4 Further screening example: infinitely many D -optimal designs

Stallrich et al. (2023) provide several examples contrasting D and A in screening-design construction, including cases where D -optimality yields infinitely many solutions with different variance properties. Our factorization provides a compact lens for these phenomena.

In Stallrich et al. (2023, Figure 1), a design for $n = 7$ runs and $k = 5$ factors is shown to be simultaneously A - and D -optimal under a main-effects working model with an intercept. The published A -optimal design has $x_{14} = x_{15} = 0$, and Stallrich et al. (2023) show that changing either of these two entries to any value in $[-1, 1]$ yields another D -optimal design, but with equal or larger variances. Thus the A -optimal design is unique, even though it sits inside an infinite family of D -optimal ties.

Table 3 reports the factorization quantities for the published A -optimal design and for two alternative D -optimal designs obtained by setting $(x_{14}, x_{15}) = (1, 1)$ and $(x_{14}, x_{15}) = (-1, 1)$. As in Section 3, we report D_{eff} , A_{eff} , and G_{eff} as relative efficiencies (larger is better). All three are an exact tie in D , so differences in A are explained entirely by the sphericity index \mathcal{S} . Figure 2b shows the corresponding ordered normalized covariance spectra.

Again the spectral ordering matches the variance diagnostics. The published D/A -optimal design has the flattest covariance spectrum and the largest sphericity, while the two alternative D ties progressively inflate the largest covariance directions. That loss of spectral balance is mirrored by lower A_{eff} and, especially, by much lower G_{eff} .

Design	D_{eff}	A_{eff}	G_{eff}	$\mathcal{S}(C)$	$p/D(X)$
D/A-opt	90.71	85.71	57.14	0.945	0.94
D-opt (1,1)	90.71	76.19	28.57	0.840	0.94
D-opt (-1,1)	90.71	80.67	42.86	0.889	0.94

Table 3: [Stallrich et al. \(2023, Figure 1\)](#): relative efficiencies and sphericity for three D -optimal ties.

5 Space-filling post-screening: MaxPro divided by sphericity

Space-filling designs are commonly generated without specifying a target linear model. For example, fast flexible filling (FFF) designs, as implemented in JMP, are constructed to fill factor space efficiently, often using a maximum projection (MaxPro) objective ([Joseph et al., 2015](#); [Lekivetz and Jones, 2015](#)). If a low-order working model is also of interest (e.g., screening or response-surface terms), then (6) suggests a natural way to add a shape preference without abandoning the space-filling objective. U-Bridge designs provide a stronger, model-targeting bridge for selecting from space-filling candidates ([Jones and Steinberg, 2025](#)); the present proposal is intentionally lighter and retains the primary spacing objective.

5.1 From inverse D to MaxPro: a sphericity-weighted post-screen

Equation (6) can be read as

$$(\text{primary criterion}) \times (\text{shape penalty}) \quad \text{with} \quad \text{primary criterion} = 1/D, \text{ shape penalty} = 1/\mathcal{S}.$$

This suggests a broader template: retain a primary criterion that controls the main design objective, then use sphericity as a secondary shape adjustment. When the primary goal is space filling, it is natural to let MaxPro take the role of the primary spacing criterion to be minimized and to treat \mathcal{S} as a model-based shape reward (larger \mathcal{S} implies more uniform information over coefficient directions). This motivates the composite score

$$\text{score}(\xi) := \frac{\text{MaxPro}(\xi)}{\mathcal{S}(\xi)} \tag{10}$$

for a design ξ in a candidate pool, where $\mathcal{S}(\xi)$ is computed under a specified working model. Minimizing MaxPro/ \mathcal{S} rewards designs that are both space filling and spectrally well balanced under the model.

We view (10) as a post-screen rather than a stand-alone global optimality criterion. Downselecting by sphericity alone would be blind to geometric coverage and could, in principle, prefer candidates that are spectrally balanced under the working model but comparatively poor in space-filling spread. A natural question is whether direct optimization via a local row-exchange heuristic can substitute for the repeated-FFF post-screen. Our preliminary experiments support the caution above: maximizing \mathcal{S} alone concentrated many points near the center of the region. Row exchange aimed at reducing MaxPro/ \mathcal{S} did improve weaker candidates in the pool, but did not bring them up to the level of the best candidate identified by the post-screen; when started from that best candidate, it produced only minor further changes. This suggests that the post-screen is effective at identifying a strong starting design, and that the candidate-pool variation captured by the composite score is not easily recovered by local search alone.

In many practical workflows, a space-filling design is generated once and the user performs only a light visual check that the points appear reasonably scattered. Our suggestion is to run

Design	D_{eff}	A_{eff}	G_{eff}	$\mathcal{S}(C)$	$p/D(X)$	MaxPro	MaxPro/ \mathcal{S}
Min MaxPro/ \mathcal{S}	27.61	19.51	32.79	0.707	1.09	26.82	37.96
Max MaxPro/ \mathcal{S}	23.21	14.63	16.35	0.630	1.29	30.05	47.66

Table 4: FFF candidate pool ($n = 20$, $[-1, 1]^2$): two designs at the extremes of MaxPro/ \mathcal{S} .

the space-filling construction multiple times (e.g., different random seeds), then select among the resulting candidates using the composite score MaxPro/ \mathcal{S} (Eq. 10) as a secondary screen; more conservatively, one can first restrict attention to a competitive MaxPro band (for example, the best 10%) and then choose the design with the largest \mathcal{S} within that band.

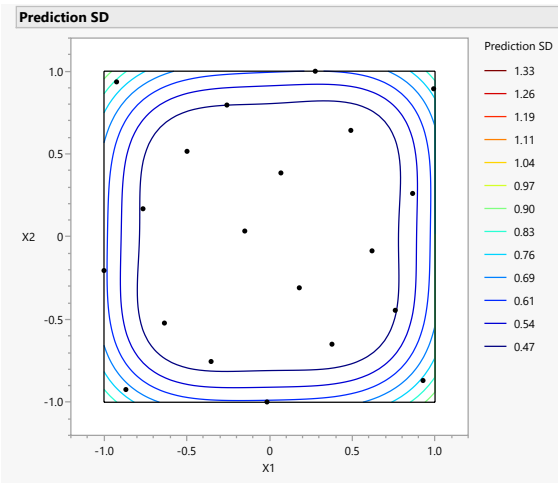
5.2 Illustration with an FFF candidate pool

We generate a pool of $N = 500$ JMP FFF candidates (same run size and factor ranges), record the MaxPro objective for each candidate, and compute \mathcal{S} under a quadratic response-surface working model. Across this pool, the sample correlation between MaxPro and \mathcal{S} is -0.16 . This weak association indicates that, even among candidates produced by the same FFF algorithm, better MaxPro values do not automatically imply better working-model balance. This leaves room for a meaningful post-screen among designs that are already competitive on MaxPro.

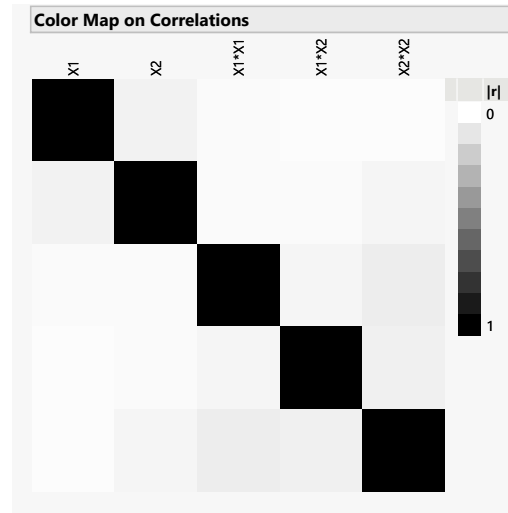
To visualize what working-model sphericity is capturing, we use the relative prediction-variance function $v(x) = f(x)^\top (X^\top X)^{-1} f(x)$ under the quadratic working model. Its maximum over the region is the G criterion (worst relative prediction variance) (Myers et al., 2016). For candidates that are comparable on the spacing objective, contours of the prediction standard deviation $\sqrt{v(x)}$ provide a direct view of how prediction uncertainty varies across factor space. For interpretability, Figure 3 contrasts two candidates drawn from the extremes of MaxPro/ \mathcal{S} within the pool. The left panels overlay $\sqrt{v(x)}$ contours on the design points, while the right panels show the correlation matrix of $\hat{\beta}$ under the working model. Both displays reflect the same underlying spectral behavior: smaller \mathcal{S} corresponds to a more uneven covariance spectrum, which concentrates uncertainty into a few directions. Table 4 summarizes the associated metrics and includes the composite MaxPro/ \mathcal{S} score from (10).

The lower-MaxPro/ \mathcal{S} design is better on every reported criterion in Table 4. Its prediction-standard-deviation contours are more even across the region, and its coefficient-correlation heatmap is visibly less structured, both consistent with its larger sphericity. The higher-MaxPro/ \mathcal{S} design shows stronger correlation and more uneven contours, illustrating that the same FFF algorithm can produce noticeably different working-model support across random seeds.

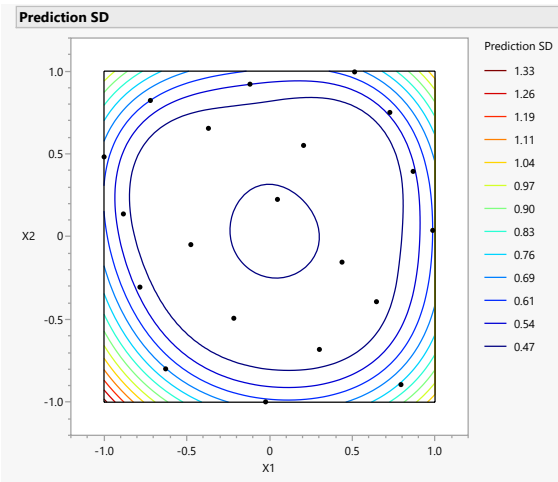
The same post-screen may also be useful when space-filling initial designs are used to support low-order surrogate modeling, for example in Bayesian optimization (Shahriari et al., 2016) and self-validated ensemble model (SVEM)-based workflows (Karl, 2026).



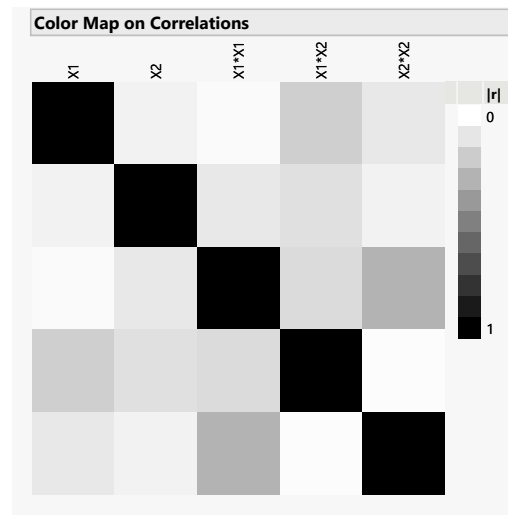
(a) Low MaxPro/ \mathcal{S} : design points with prediction standard deviation contours.



(b) Low MaxPro/ \mathcal{S} : correlation heatmap of $\hat{\beta}$.



(c) High MaxPro/ \mathcal{S} : design points with prediction standard deviation contours.



(d) High MaxPro/ \mathcal{S} : correlation heatmap of $\hat{\beta}$.

Figure 3: FFF pool illustration: extremes of MaxPro/ \mathcal{S} .

6 Extensions via Kiefer’s Phi-class and sphericity profiles

This paper has focused on A - and D -optimality, but the same scale/shape separation extends naturally to a broader framework.

6.1 Kiefer’s Φ -class and scale/shape separation

Following [Kiefer \(1974\)](#) and [Sagnol \(2013, Appendix A.2\)](#), let C be a positive definite information matrix with eigenvalues $\mu_1, \dots, \mu_p > 0$. For an index $r \in [-\infty, 1]$, define Kiefer’s Φ -criteria by

$$\Phi_r(C) = \begin{cases} \min_i \mu_i, & r = -\infty, & E\text{-criterion,} \\ \left\{ \frac{1}{p} \operatorname{tr}(C^{-1}) \right\}^{-1} = \frac{p}{A(X)}, & r = -1, & A\text{-criterion,} \\ \left\{ \frac{1}{p} \operatorname{tr}(C^r) \right\}^{1/r}, & r \in (-\infty, 1], r \notin \{-1, 0\}, \\ \{\det(C)\}^{1/p}, & r = 0, & D\text{-criterion.} \end{cases} \quad (11)$$

Here C^r is defined spectrally, so that $\operatorname{tr}(C^r) = \sum_{i=1}^p \mu_i^r$. Thus Φ_r is a generalized mean of the information eigenvalues: as r decreases, the criterion puts progressively more weight on the smaller information directions. At the upper end, $\Phi_1(C) = \operatorname{tr}(C)/p$ is simply the arithmetic mean of the information spectrum; unlike D -optimality ($r = 0$), which uses the geometric mean and therefore depends only on confidence-ellipsoid volume, Φ_1 is less sensitive to weak directions and has no direct volume interpretation.

Normalizing by the D scale yields the same scale/shape factorization,

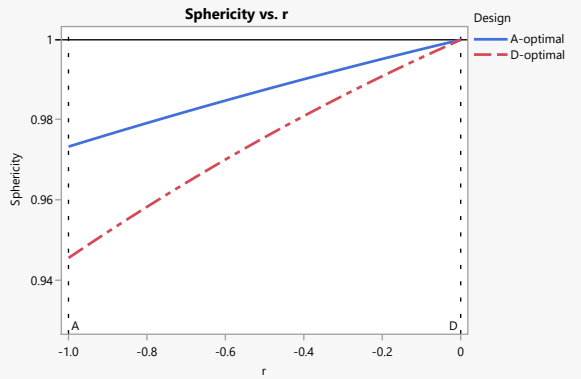
$$\mathcal{S}_r(C) := \frac{\Phi_r(C)}{\Phi_0(C)} \quad \Rightarrow \quad \Phi_r(C) = \Phi_0(C) \mathcal{S}_r(C). \quad (12)$$

The ratio $\mathcal{S}_r(C)$ is scale free, since replacing C by cC for any $c > 0$ multiplies both numerator and denominator by the same factor ([Sagnol, 2013, Appendix A.2](#)). It therefore depends only on spectral balance. For $r < 0$, $0 < \mathcal{S}_r(C) \leq 1$, with equality if and only if the eigenvalues are all equal. In particular, $\mathcal{S}_0(C) \equiv 1$, so the D criterion uses only the determinant scale $\Phi_0(C)$ and is blind to spectral shape beyond the determinant. Thus Kiefer’s parameter r provides a continuous bridge from D toward criteria that increasingly penalize weak information directions, with A appearing as the case $r = -1$.

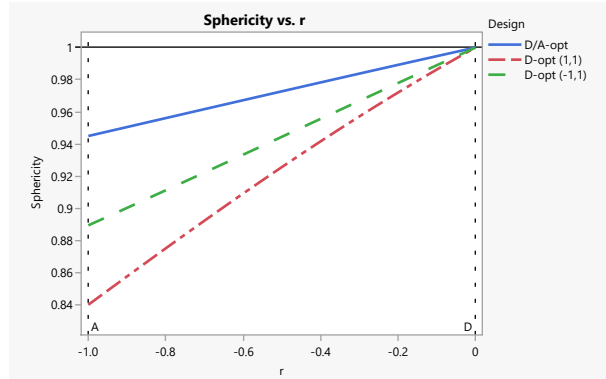
6.2 Sphericity profiles

Our sphericity index is the $r = -1$ case, $\mathcal{S}(C) = \mathcal{S}_{-1}(C)$, and (6) can be read as “ A equals inverse- D scale divided by sphericity.” A useful diagnostic is the sphericity profile $\mathcal{S}_r(C)$ as a function of r over a range such as $r \in [-1, 0]$. This provides a shape-only view that connects D ($r = 0$) to more curvature-sensitive criteria. Figure 4a shows an example for the published D tie of [Jones et al. \(2021, Example 2\)](#), and Figure 4b shows the profile for the example of [Stallrich et al. \(2023\)](#). In both cases the ordering is stable over $r < 0$, so the preference for the better-balanced design is not an artifact of the single choice $r = -1$.

The same viewpoint suggests possible research directions: one could replace $\mathcal{S}_r(C)$ by other measures of departure from sphericity, such as the standard deviation of normalized eigenvalues, or a geometric penalty linked to surface area via an isoperimetric ratio. At present, however, the determinant–trace choice is appealing because it is both interpretable—in the A case it ties directly



(a) Jones et al. (2021, Example 2).



(b) Stallrich et al. (2023, Figure 1).

Figure 4: Sphericity profiles $\mathcal{S}_r(C)$ as a function of r .

to Mauchly’s W —and computationally trivial to evaluate from eigenvalues, unlike surface-area penalties that would typically require numerical approximation. Because $\mu_i = s_i^2$, all of these expressions can also be computed from the singular values of X ; if X is rank deficient, some $s_i = 0$, clarifying why the classical A and D criteria degenerate.

7 Conclusion

The factorization (6) is algebraically simple and practically useful: it separates the part of A that is already captured by D from the part that D does not see. Once determinant-based scale is fixed, the remaining variation in A is a matter of spectral balance, summarized by \mathcal{S} .

The decomposition also gives a clear interpretation of the two components. D controls overall information scale, equivalently the confidence-ellipsoid volume scale, whereas \mathcal{S} controls shape. That distinction is exactly what allows A to discriminate among designs that are tied, or nearly tied, on D . The examples in Sections 3–4 make this visible: higher sphericity aligns with flatter covariance spectra, better A_{eff} , and in these cases markedly better G_{eff} . Section 5 shows that the same idea remains useful beyond exact determinant ties: keep MaxPro as the primary spacing criterion, then use sphericity to choose the better-balanced design within the competitive set.

More broadly, the Kiefer-class extension shows that the same separation between scale and spectral balance persists beyond the A case. Among designs that are already competitive on a primary criterion, especially among D ties or near ties, sphericity indicates whether the information is well balanced under the working model. In JMP this quantity is immediately available as $\mathcal{S} = A_{\text{eff}}/D_{\text{eff}}$.

Data availability statement

The design matrices analyzed in Sections 3–4 are taken from the cited publications. The scripts used to compute the reported criteria and generate the figures and tables are included in the online supplementary material. Additional data and materials that support the findings of this study are available from the corresponding author upon request.

Disclosure of interest

The authors report no competing interests.

Funding

No funding was received.

Declaration of generative AI and AI-assisted technologies in the manuscript preparation process

During the preparation of this work the first author used GPT-5.2 Pro to proofread/reword text and refine LaTeX formatting. After using this tool, the author reviewed the content and takes full responsibility for the content of the published article.

References

- Peter Goos. *The Optimal Design of Blocked and Split-Plot Experiments*. Springer, New York, 2002.
- David A. Harville. *Matrix Algebra from a Statistician's Perspective*. Springer, New York, 1997.
- Bradley Jones and David M. Steinberg. Unrestricted bridge (U-bridge) designs for settings with non-deterministic data. *Quality and Reliability Engineering International*, 41(8):3405–3414, 2025. doi: 10.1002/qre.70050.
- Bradley Jones, Katherine Allen-Moyer, and Peter Goos. A-optimal versus D-optimal design of screening experiments. *Journal of Quality Technology*, 53(4):369–382, 2021. doi: 10.1080/00224065.2020.1757391.
- V. Roshan Joseph, Evren Gul, and Shan Ba. Maximum projection designs for computer experiments. *Biometrika*, 102(2):371–380, 2015. doi: 10.1093/biomet/asv002.
- Andrew T. Karl. SVEMnet: An R package for self-validated elastic-net ensembles and multi-response optimization in small-sample mixture–process experiments. *Chemometrics and Intelligent Laboratory Systems*, 271:105660, 2026. ISSN 0169-7439. doi: 10.1016/j.chemolab.2026.105660.
- J. Kiefer. General equivalence theory for optimum designs (approximate theory). *The Annals of Statistics*, 2(5):849–879, 1974. doi: 10.1214/aos/1176342810.
- Ryan Lekivetz and Bradley Jones. Fast flexible space-filling designs for nonrectangular regions. *Quality and Reliability Engineering International*, 31(5):829–837, 2015. doi: 10.1002/qre.1640.
- John W. Mauchly. Significance test for sphericity of a normal n -variate distribution. *The Annals of Mathematical Statistics*, 11(2):204–209, 1940. doi: 10.1214/aoms/1177731915.
- Raymond H. Myers, Douglas C. Montgomery, and Christine M. Anderson-Cook. *Response Surface Methodology: Process and Product Optimization Using Designed Experiments*. Wiley, 4 edition, 2016.
- B. N. Nagarsenker and K. C. S. Pillai. The distribution of the sphericity test criterion. *Journal of Multivariate Analysis*, 3(2):226–235, 1973. doi: 10.1016/0047-259X(73)90025-0.
- Guillaume Sagnol. Approximation of a Maximum-Submodular-Coverage problem involving spectral functions, with application to experimental designs. *Discrete Applied Mathematics*, 161(1):258–276, 2013. doi: 10.1016/j.dam.2012.07.016.
- SAS Institute Inc. Design efficiency, 2025. JMP Documentation, Design of Experiments Guide: Evaluate Designs. Publication date 07/15/2025. Available at <https://www.jmp.com/support/help/en/19.0/#page/jmp/design-efficiency.shtml#ww661228> (accessed 2026-02-26).
- Bobak Shahriari, Kevin Swersky, Ziyu Wang, Ryan P. Adams, and Nando de Freitas. Taking the human out of the loop: A review of Bayesian optimization. *Proceedings of the IEEE*, 104(1): 148–175, 2016. doi: 10.1109/JPROC.2015.2494218.
- Jonathan Stallrich, Katherine Allen-Moyer, and Bradley Jones. D- and A-optimal screening designs. *Technometrics*, 65(4):492–501, 2023. doi: 10.1080/00401706.2023.2183262.